RSC Advances

PAPER

Facile hydrothermal synthesis of SnO_2/C microspheres and double layered core–shell SnO_2 microspheres as anode materials for Li-ion secondary batteries†

Cite this: *RSC Adv.*, 2014, **4**, 25189

Mingbo Wu,*[a] Jun Liu,[a] Minghui Tan,[a] Zhongtao Li,[a] Wenting Wu,[a] Yanpeng Li,[a] Huaiping Wang,[a] Jingtang Zheng[a] and Jieshan Qiu*[b]

Received 17th January 2014
Accepted 27th May 2014

DOI: 10.1039/c4ra00477a

www.rsc.org/advances

SnO_2/C microspheres and double layered core–shell SnO_2 microspheres have been synthesized by a facile hydrothermal method with a post heat-treatment. The soluble starch used as carbon source and the mass ratio of starch to $SnCl_4 \cdot 5H_2O$ play key roles in the formation of SnO_2/C microspheres, and the hydrothermal synthesis mechanism of SnO_2/C microspheres has been proposed. SnO_2/C-1.0 microspheres (the mass ratio of soluble starch to $SnCl_4 \cdot 5H_2O$ is 1 : 1) with good spherical shape and 34.91 wt% of SnO_2 exhibit superior rate capability and cyclic stability, while double layered core–shell SnO_2 microspheres show improved electrochemical performance compared to SnO_2 particles. The electrode based on SnO_2/C-1.0 microspheres delivers a reversible discharge capacity of 568 mA h g^{-1} at a constant current density of 100 mA g^{-1} in the second cycle, and 379 mA h g^{-1} (67% retention) is retained after the 50th cycle, suggesting SnO_2/C microspheres are promising candidates for energy storage.

1 Introduction

Li-ion batteries (LIBs) have attracted significant attention due to their high work voltage, high energy density, high energy efficiency, long cycle life and environmentally friendly nature.[1–3] Such outstanding advantages make them good candidates for applications in hybrid electric vehicles, portable electronics, large industrial equipment, and other renewable energy storage.[1,3,4] The electrochemical properties of LIBs largely depend on their electrode materials, currently used commercial graphite anodes have a limited theoretical capacity of 372 mA h g^{-1}, so alternative materials are highly desired.[3,5,6]

SnO_2 as LIBs anode has attracted much attention on the basis of its higher theoretical specific capacity (790 mA h g^{-1}) than that of graphite.[7,8] However, a large volume change (about 300%) occurs in SnO_2 anode during lithium insertion/extraction processes, which causes pulverization of anode particles and loss of contact with current collector, resulting in poor electrochemical performance.[5,7–9] In order to improve the electrochemical properties of SnO_2-based anodes, lots of effective ways to regulate the composition or structure of the electrode material have been reported. SnO_2/carbon composites,[10,11] hollow or core–shell SnO_2/carbon composites,[7,12,13] SnO_2/graphene composites,[14–18] and hollow or yolk–shell SnO_2 spheres[8,9,19–22] have been prepared and used as anode materials for LIBs in recent years. Although all of above mentioned SnO_2-based materials have improved electrochemical properties, the complex technologies or tedious multi-step methods used in their preparation process hinder their widely industrial applications.

In this work, a facile hydrothermal method of synthesizing SnO_2/C microspheres and double layered core–shell SnO_2 microspheres with a post heat-treatment was proposed. The mechanism of the hydrothermal formation of SnO_2/C microspheres was discussed, and the electrochemical performances of SnO_2/C microspheres and core–shell-structured SnO_2 microspheres in LIBs were investigated.

2 Experimental

2.1 Sample preparation

The overall synthetic procedure is described in Fig. 1. $SnCl_4 \cdot 5H_2O$ (AR, Sinopharm Chemical Reagent Co., Ltd.) and soluble starch (AR, Sinopharm Chemical Reagent Co., Ltd.) were selected as the precursors of SnO_2 and carbon material, respectively. Soluble starch and $SnCl_4 \cdot 5H_2O$ were fully dispersed in deionized water with the mass ratio of soluble starch, $SnCl_4 \cdot 5H_2O$ and water at 1 : 1 : 3.37. 80 mL of the resulting mixture was transferred into a 100 mL Teflon-lined

[a]*State Key Laboratory of Heavy Oil Processing, China University of Petroleum, Qingdao 266580, China. E-mail: wumb@upc.edu.cn*

[b]*Carbon Research Laboratory, State Key Lab of Fine Chemicals, School of Chemical Engineering, Dalian University of Technology, Dalian 116024, China. E-mail: jqiu@dlut.edu.cn*

† Electronic supplementary information (ESI) available. See DOI: 10.1039/c4ra00477a

This journal is © The Royal Society of Chemistry 2014

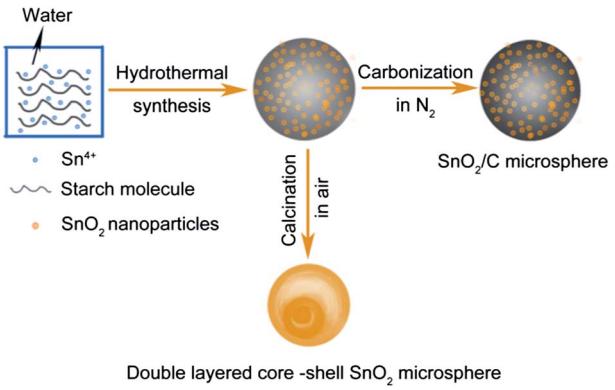

Fig. 1 Schematic formation processes of SnO_2/C microspheres and double layered core–shell SnO_2 microspheres.

stainless steel autoclave, and then heated at 190 °C for 12 h. Dark precipitates were collected and washed with distilled water and ethanol, and finally dried in an oven at 100 °C for 12 h, thus, primary SnO_2/C microspheres were obtained. The primary SnO_2/C microspheres were then carbonized at 500 °C for 3 h under nitrogen atmosphere to prepare SnO_2/C microspheres (named SnO_2/C-1.0). For the preparation of core–shell-structured SnO_2 microspheres, the primary SnO_2/C microspheres were calcined in air at 600 °C for 3 h.

2.2 Characterization of samples

The surface morphology and microstructure of obtained samples were investigated by field emission scanning electron microscopy (FE-SEM, S4800, Japan) and transmission electron microscopy (TEM, JEM-2100UHR, Japan). The phase composition and crystalline properties of as-prepared products were characterized by X-ray diffraction (XRD, X'Pert PRO MPD, Netherlands).

2.3 Preparation of electrodes and electrochemical measurements

The obtained sample was mixed with carbon black and polyvinylidenefluoride (PVDF) binder to form slurry at the weight ratio of 8 : 1 : 1. *N*-methyl-2-pyrrolidone was used as the solvent. The electrode was prepared by casting the slurry onto copper foil and drying in a vacuum oven at 120 °C for 12 h. CR2032 coin cells were assembled in an Ar-filled glove-box with lithium foil as the counter electrode, and polypropylene film (Celgard 2400) as the separator. The electrolyte was 1 M $LiPF_6$ dissolved in 1 : 1 volume ratio with ethylene carbonate/dimethyl carbonate (EC/DMC). The electrochemical properties of the electrodes were studied by cyclic voltammetry and galvanostatic charge–discharge on Arbin battery test system (BT2000, Arbin Instruments, USA). Cyclic voltammetry was performed in the potential range from 0.01 to 3 V (*vs.* Li^+/Li) at a scan rate of 0.2 mV s^{-1}. Galvanostatic charge–discharge measurements were carried out between 0.01 and 3 V (*vs.* Li^+/Li) at different current densities.

3 Results and discussion

Fig. 2 shows the XRD patterns of SnO_2/C-1.0 microspheres and double layered core–shell SnO_2 microspheres. The pattern of double layered core–shell SnO_2 microspheres can be indexed well as SnO_2. The four dominant broad peaks (110), (101), (211), and (301) in XRD pattern of double layered core–shell SnO_2 microspheres are attributed to the SnO_2 phase (JCPDS no. 41-1445), indicating the formation of tetragonal SnO_2 nanocrystals. Some weak peaks of metallic Sn are exhibited in the XRD pattern of SnO_2/C-1.0 microspheres, indicating little amount of SnO_2 were reduced to metallic Sn by carbon during the heat-treated process.[10]

From SEM images shown in Fig. 3(A) and (B), we can see that SnO_2/C-1.0 microspheres are mainly in spherical shape with particle size ranging from 1 to 5 μm, and the spheres are solid. Energy dispersive spectrometer (EDS, S4800, Japan) analysis was used to evaluate the composition of the smaller particles in Fig. 3(A), Sn, O and C are found in the smaller particles (see Fig. S1 in the ESI†), implying that the smaller particles are the composite of SnO_2 and carbon. Double layered core–shell SnO_2

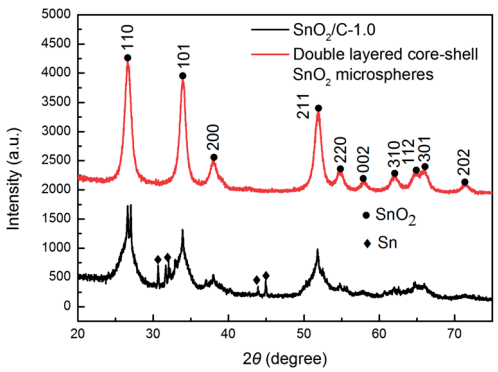

Fig. 2 XRD patterns of SnO_2/C-1.0 microspheres and double layered core–shell SnO_2 microspheres.

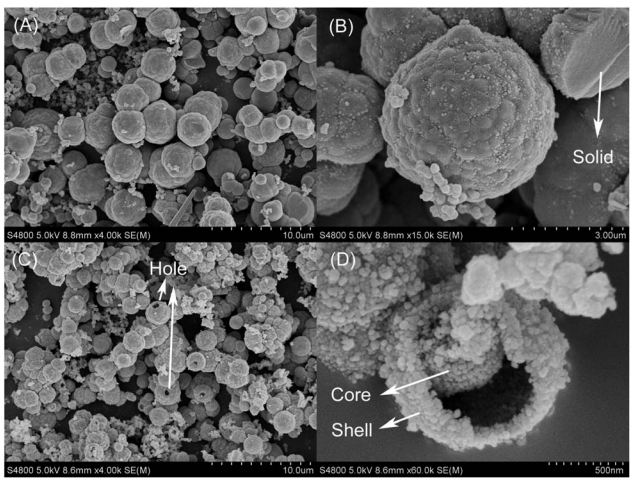

Fig. 3 SEM images of SnO_2/C-1.0 microspheres (A and B) and double layered core–shell SnO_2 microspheres (C and D).

 This journal is © The Royal Society of Chemistry 2014

microspheres in Fig. 3(C) are distinctly smaller than SnO_2/C-1.0 microspheres in Fig. 3(A) and there is an open hole on the surface of most double layered core–shell SnO_2 microsphere, which was brought by the burning of carbon and polymeric molecules in air and inner gases were evacuated during calcination process.[19,21] Through the hole (Fig. 3(D)), we can clearly see that the microsphere is composed of a thin outer shell and an inside smaller sphere, indicating the core–shell structure of double layered core–shell SnO_2 microsphere.

TEM image in Fig. 4(A) shows that SnO_2/C-1.0 microspheres are solid spheres and SnO_2 nanoparticles are uniformly dispersed in carbon matrix. Fig. 4(B) reveals the double layered core–shell structure of double layered core–shell SnO_2 microspheres. The high resolution TEM (HR-TEM) image of double layered core–shell SnO_2 microspheres, as shown in Fig. 4(C), exhibits clear lattice fringes separated by 0.33 nm and 0.26 nm, which are in good agreement with the (110) and (101) planes of rutile SnO_2, respectively. The corresponding ring-like selected-area electron diffraction (SAED) pattern shown in Fig. 4(D) indicates that the double layered core–shell SnO_2 microspheres are polycrystalline, and the diffraction rings of the pattern can be completely indexed to planes of rutile SnO_2, which also can be seen from XRD pattern in Fig. 2.

The N_2 adsorption–desorption isotherms and pore size distribution of SnO_2/C-1.0 microspheres, double layered core–shell SnO_2 microspheres and SnO_2 particles prepared without starch are shown in Fig. S2 (see the ESI†). Fig. S2(A)† shows that SnO_2/C-1.0 microspheres are microporous carbon evidenced by the type I isotherm while the pores in double layered core–shell SnO_2 microspheres and SnO_2 particles are mainly mesopores seen from the obvious hysteresis loops, which also can be clearly confirmed by the pore size distribution in Fig. S2(B).† The BET surface area of SnO_2/C-1.0 microspheres, double layered core–shell SnO_2 microspheres and SnO_2 particles is 263 $m^2\ g^{-1}$, 46 $m^2\ g^{-1}$ and 24 $m^2\ g^{-1}$, respectively.

To evaluate the weight percentage of SnO_2 in SnO_2/C-1.0, the as-synthesized composite was calcined in air at 600 °C for 3 h, the obtained powders were white, indicating the carbon had been completely burned out and the residue was SnO_2. Thus the content of SnO_2 in SnO_2/C-1.0 microspheres is calculated to be 34.91 wt%. For comparison with SnO_2/C-1.0 microspheres (the mass ratio of soluble starch, $SnCl_4 \cdot 5H_2O$ and water was 1 : 1 : 3.37), SnO_2/C composites were prepared with the mass ratios of soluble starch, $SnCl_4 \cdot 5H_2O$ and water at 1 : 1.5 : 3.37 and 1 : 0.5 : 3.37, which were termed as SnO_2/C-1.5 and SnO_2/C-0.5, respectively. The contents of SnO_2 in SnO_2/C-1.5 and SnO_2/C-0.5 are about 34.62 wt% and 39.25 wt%, respectively. It is interesting that the content of SnO_2 in SnO_2/C decreases with the increasing amount of added $SnCl_4 \cdot 5H_2O$, more work is needed in future to explain this trend. From the SEM images of SnO_2/C-1.5 and SnO_2/C-0.5 (see Fig. S3 in the ESI†), we can see that both SnO_2/C-1.5 and SnO_2/C-0.5 show bad spherical shapes, indicating that there is a limitation of the amount of $SnCl_4 \cdot 5H_2O$ added and a suitable weight percentage of SnO_2 to keep the microsphere morphology.

To understand the role of starch molecule in the hydrothermal synthesis process of SnO_2/C microspheres, primary carbon microspheres and SnO_2 particles were obtained by the same hydrothermal method. The synthesis procedure of primary carbon microspheres or SnO_2 particles was as same as that of primary SnO_2/C microspheres except without addition of $SnCl_4 \cdot 5H_2O$ or soluble starch. From SEM images of the primary carbon microspheres (Fig. 5(A)) and the primary SnO_2/C microspheres (Fig. 5(B)), we can clearly see that the primary carbon microspheres have relatively smooth surface while primary SnO_2/C microspheres have raspberry-like surface, which may be due to the SnO_2 nanoparticles bedded in the primary SnO_2/C microspheres, see TEM image in Fig. 5(C). Fig. 5(D) shows the primary SnO_2 particles synthesized without addition of soluble starch, irregular aggregation of nanoparticles is observed and no obvious microsphere was obtained, implying the starch molecules do play an important role in the formation of SnO_2/C microspheres.

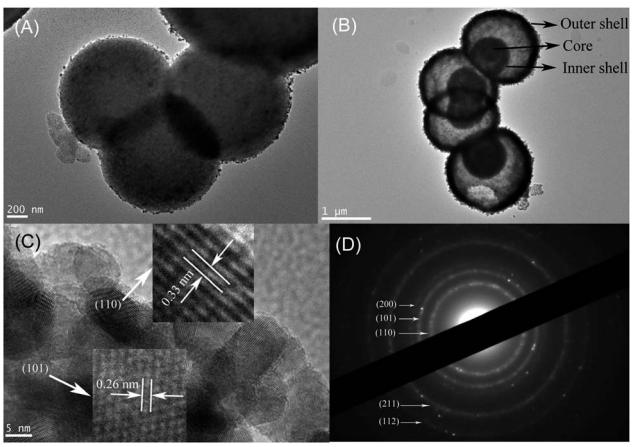

Fig. 4 TEM images of SnO_2/C-1.0 microspheres (A) and double layered core–shell SnO_2 microspheres (B), HR-TEM image (C) and SAED pattern (D) of double layered core–shell SnO_2 microsphere.

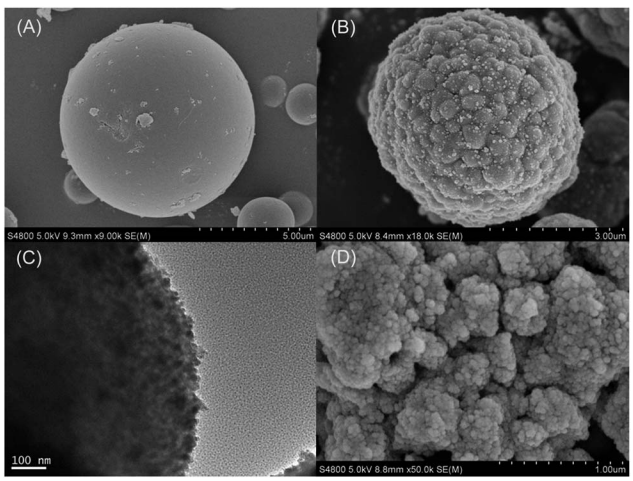

Fig. 5 SEM images of the primary carbon microsphere (A), the primary SnO_2/C microsphere (B) and primary SnO_2 particles (D) and TEM image of the primary SnO_2/C microsphere (C).

Hydrothermal synthesis mechanism of carbon microsphere from saccharides (starch,[23–25] cellulose,[26] sucrose,[23,24] glucose,[23,24,27] fructose[27]) have been reported in references. Based on these references and our experimental results, we propose a possible hydrothermal synthesis mechanism of SnO_2/C microspheres, as show in Fig. 6. In the initial stage, the starch hydrolyzes and glucose molecules are produced. At the same time, hydrolysis of $SnCl_4 \cdot 5H_2O$ results in numerous primary SnO_2 hydrate nanoparticles in solution, and these SnO_2 hydrate nanoparticles are immediately entrapped by glucose molecules due to OH groups on glucose molecules.[19,25,28] The glucose molecules adsorbed on the surface of SnO_2 nanoparticles prevent the direct contact among SnO_2 nanoparticles, thus aggregation of SnO_2 nanoparticles is avoided. Driven by the reduction of overall surface energy, SnO_2 nanoparticles entrapped by glucose molecules aggregate to form microspheres.[28,29] In the hydrothermal environment, dehydration and polymerization reactions can take place among glucose molecules, thus the primary SnO_2/C microspheres are formed. As for the formation mechanism of double layered core–shell SnO_2 microspheres, the burning of carbon and polymeric molecules in air at 600 °C and the evacuation of inner gases during calcination process make the core–shell structure of double layered core–shell SnO_2 microspheres.[20,21]

Fig. 7 shows the initial 5 cyclic voltammograms of electrodes prepared from SnO_2/C-1.0 microspheres and double layered core–shell SnO_2 microspheres at a scan rate of 0.2 mV s^{-1} between 0.01 and 3 V. Two reduction peaks are observed in the first cathodic scan in both Fig. 7(A) and (B). The cathodic peaks around 0.6 V can be attributed to the formation of the solid electrolyte interface (SEI) layer and the reduction of SnO_2 to form Sn and Li_2O, the peak at low potential (<0.5 V) corresponds to the formation of Li–Sn alloy,[20,30–32] the reactions as follows:

$$Li^+ + e^- + \text{electrolyte} \rightarrow \text{SEI (Li)} \quad (1)$$

$$4Li^+ + SnO_2 + 4e^- \rightarrow 2Li_2O + Sn \quad (2)$$

$$xLi^+ + Sn + xe^- \leftrightarrow Li_xSn\ (0 \leq x \leq 4.4) \quad (3)$$

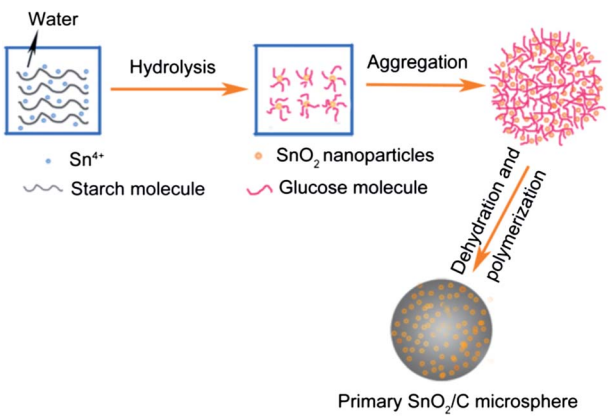

Fig. 6 Hydrothermal synthesis mechanism of SnO_2/C microspheres.

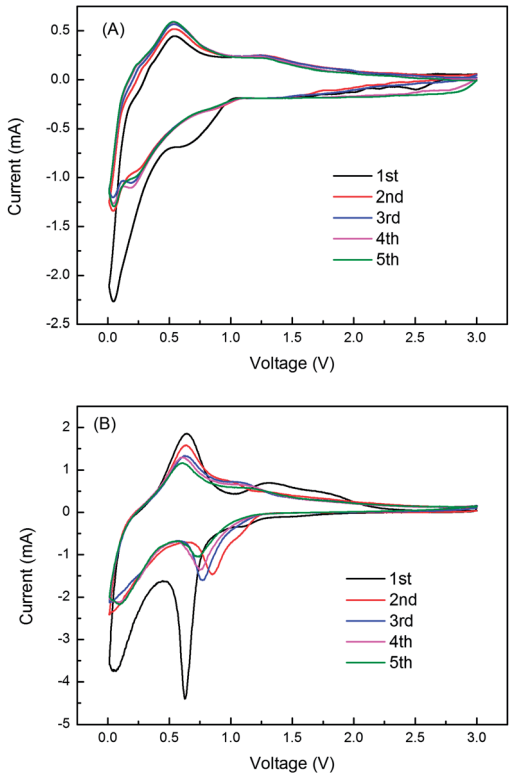

Fig. 7 Cyclic voltammograms of SnO_2/C-1.0 (A) and double layered core–shell SnO_2 microspheres (B).

The oxidation peak at 0.54 V can be assigned to the dealloying of Li_xSn, while the weak oxidation at 1.25 V is due to the partly reversible reaction (2). The obvious difference between the first cycle and the second cycle is due to irreversible reactions (1) and (2), leading to initially irreversible capacity loss.[13,15] From the 2nd cycle to the 5th cycle, the curves of SnO_2/C-1.0 microspheres become similar, suggesting better stability of SnO_2/C-1.0 microspheres than that of double layered core–shell SnO_2 microspheres.

For comparison, above mentioned primary SnO_2 particles were calcined in air at 600 °C for 3 h, and the obtained SnO_2 particles were used as anode material for LIBs. The cycling performances and rate capabilities of SnO_2/C-1.0 microspheres, double layered core–shell SnO_2 microspheres and SnO_2 particles are shown in Fig. 8(A) and (B), respectively. In Fig. 8(A), SnO_2/C-1.0 microspheres, double layered core–shell SnO_2 microspheres and SnO_2 particles deliver reversible discharge capacities of 568 mA h g^{-1}, 935 mA h g^{-1}, 825 mA h g^{-1} at a constant current density of 100 mA g^{-1} in the 2nd cycle, respectively, which are much higher than the theoretical capacity of graphite (372 mA h g^{-1}). The big initial irreversible capacity loss in the 1st cycle is due to the formation of the SEI layer and the reduction of SnO_2 to form Sn and Li_2O.[10,12,20,33] The higher capacities of double layered core–shell SnO_2 microspheres and SnO_2 particles than 790 mA h g^{-1} of the theoretical value can be attributed to the reversible polymerization of electrolyte[9,34] and the partly reversible reaction (2). The higher capacity of double layered core–shell SnO_2 microspheres than

 This journal is © The Royal Society of Chemistry 2014

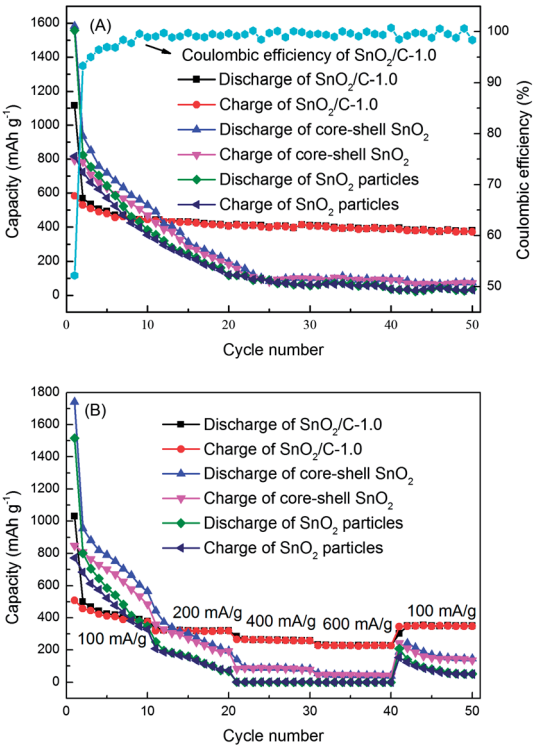

Fig. 8 The cycling performances (A) and rate capabilities (B) of the electrodes.

that of SnO_2 particles may due to the increased contact area between the electrolyte and the electrode of the core–shell structure. Double layered core–shell SnO_2 microspheres and SnO_2 particles have high capacities in the initial several cycles, but the capacity decreases quickly due to pulverization of electrode materials.[33,35] The discharge capacities of double layered core–shell SnO_2 microspheres and SnO_2 particles after 50 cycles are 75 mA h g^{-1} with capacity retention of 8% and 35 mA h g^{-1} with capacity retention of only 4%, respectively. The electrode produced from SnO_2/C-1.0 microspheres exhibits the best cycling performance, and its discharge capacity after 50 cycles is 379 mA h g^{-1}, 67% retention of the discharge capacity of the 2nd cycle. Fig. S4 (see the ESI†) gives the cycling performance of purely carbon microspheres, which deliver a reversible discharge capacity of only 116 mA h g^{-1} at a constant current density of 100 mA g^{-1} in the 2nd cycle, and 114 mA h g^{-1} is retained in the 50th cycle. So the high capacity of SnO_2/C-1.0 microspheres mainly comes from the SnO_2 component rather than the carbon. The coulombic efficiency of SnO_2/C-1.0 electrode is found to be around 93% for the second cycle and reaches above 98% for the 50th cycle. It is believed that carbon in SnO_2/C composite can buffer the big volume change during the charge and discharge processes and thereby enhance the structural stability of electrode.[5,10,33,36–38]

In order to make sure the difference in the electrochemical performance of composites with different SnO_2 content, the electrochemical performances of SnO_2/C-1.5 and SnO_2/C-0.5 are shown in Fig. S5 (see the ESI†). SnO_2/C-1.5 and SnO_2/C-0.5 deliver reversible discharge capacities of 156 mA h g^{-1} and 419 mA h g^{-1} at a constant current density of 100 mA g^{-1} in the second cycle, respectively. After 50 cycles, SnO_2/C-1.5 and SnO_2/C-0.5 show stable discharge capacities of 154 mA h g^{-1} and 367 mA h g^{-1}. In comparison to SnO_2/C-1.5, the higher capacity of SnO_2/C-0.5 is due to its higher SnO_2 content (the theoretical capacity of SnO_2 is 790 mA h g^{-1}). It is noted that the specific capacities of SnO_2/C-1.5 and SnO_2/C-0.5 are both lower than that of SnO_2/C-1.0 microspheres, while the SnO_2 content is SnO_2/C-0.5 > SnO_2/C-1.0 > SnO_2/C-1.5. The highest capacity of SnO_2/C-1.0 microspheres should be attributed to its good spherical shapes and suitable SnO_2 content.

Fig. 8(B) shows the capacity retention of electrodes at various current densities. Double layered core–shell SnO_2 microspheres have higher capacities than that of SnO_2 particles at all current densities, which results from the core–shell structure increasing contact area between the electrolyte and the electrode. The voids between core and shell can serve as a buffering space during lithium insertion and extraction processes.[20,22,39] It is noted that the capacities of double layered core–shell SnO_2 microspheres at higher current densities are much lower than those of SnO_2/C-1.0 microspheres, indicating the worse stability of double layered core–shell SnO_2 microspheres than that of SnO_2/C-1.0 microspheres. At the current density of 100 mA g^{-1}, the capacity of SnO_2/C-1.0 microspheres is 378 mA h g^{-1}, and keeps 320 mA h g^{-1}, 260 mA h g^{-1} and 230 mA h g^{-1} at the current densities of 200 mA g^{-1}, 400 mA g^{-1} and 600 mA g^{-1}, respectively. When the current density switches back to 100 mA g^{-1}, the capacity directly recovers to 347 mA h g^{-1}, indicating excellent rate capability of SnO_2/C-1.0 microspheres.

Morphology changes of electrodes prepared from SnO_2/C-1.0 microspheres and double layered core–shell SnO_2 microspheres after 50 cycles at the current density of 100 mA g^{-1} are shown in Fig. 9. Most SnO_2/C-1.0 microspheres in Fig. 9(A) still keep good spherical shape as a whole integration structure, demonstrating that the carbon matrix can effectively accommodate the volume change and alleviate the strain during the charge and discharge processes. However, no spheres except many pulverized particles can be observed in the SEM image of electrode based on core–shell SnO_2 microspheres (see Fig. 9(B)), suggesting the obvious pulverization of double layered core–shell SnO_2 microspheres during the charge and discharge processes. The morphology changes shown in Fig. 9 can explain the better cycling performance of SnO_2/C-1.0 microspheres than that of double layered core–shell SnO_2 microspheres.

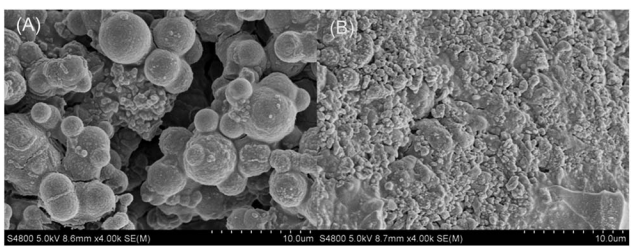

Fig. 9 SEM images of electrodes based on SnO_2/C-1.0 microspheres (A) and double layered core–shell SnO_2 microspheres (B) after 50 cycles at the current density of 100 mA g^{-1}.

4 Conclusions

In conclusion, SnO_2/C microspheres and double layered core–shell SnO_2 microspheres have been synthesized by a facile hydrothermal method with a post heat-treatment. The soluble starch used as the carbon source plays a key role in the formation of spherical SnO_2/C microspheres, and the hydrothermal mechanism of the formation of SnO_2/C microspheres has been proposed. Due to the barrier and buffer roles of carbon matrix, SnO_2/C microspheres exhibit superior rate capability and cyclic stability. The core–shell structured SnO_2 microspheres show improved electrochemical performances than SnO_2 particles, while their rate capability and cyclic stability are much worse than those of SnO_2/C microspheres. Therefore, SnO_2 nanoparticles in carbon matrix can effectively prevent the aggregation and pulverization of SnO_2 nanoparticles. It is noted that SnO_2/C microspheres in large scale can be easily prepared by this hydrothermal method, SnO_2/C microspheres may have good application future in the field of energy. This research work also can guide the preparation of metal oxide/carbon composites.

Acknowledgements

This work was supported by the National Natural Science Foundation of China (Nos. 51172285, 51372277); the Fundamental Research Funds for the Central Universities (14CX06045A, 14CX02060A).

Notes and references

1 N. S. Choi, Z. Chen, S. A. Freunberger, X. Ji, Y. K. Sun, K. Amine, G. Yushin, L. F. Nazar, J. Cho and P. G. Bruce, *Angew. Chem., Int. Ed.*, 2012, **51**, 9994–10024.
2 P. Simon and Y. Gogotsi, *Nat. Mater.*, 2008, **7**, 845–854.
3 M. V. Reddy, G. V. S. Rao and B. V. R. Chowdari, *Chem. Rev.*, 2013, **113**, 5364–5457.
4 A. Manthiram, Y. Fu and Y.-S. Su, *Acc. Chem. Res.*, 2013, **46**, 1125–1134.
5 Y. Xu, Q. Liu, Y. Zhu, Y. Liu, A. Langrock, M. R. Zachariah and C. Wang, *Nano Lett.*, 2013, **13**, 470–474.
6 A. S. Arico, P. Bruce, B. Scrosati, J. M. Tarascon and W. Van Schalkwijk, *Nat. Mater.*, 2005, **4**, 366–377.
7 X. W. Lou, C. M. Li and L. A. Archer, *Adv. Mater.*, 2009, **21**, 2536–2539.
8 X. W. Lou, Y. Wang, C. Yuan, J. Y. Lee and L. A. Archer, *Adv. Mater.*, 2006, **18**, 2325–2329.
9 W. S. Kim, Y. Hwa, J. H. Jeun, H. J. Sohn and S. H. Hong, *J. Power Sources*, 2013, **225**, 108–112.
10 J. Wang, H. Zhao, X. Liu, J. Wang and C. Wang, *Electrochim. Acta*, 2011, **56**, 6441–6447.
11 J. Read, D. Foster, J. Wolfenstine and W. Behl, *J. Power Sources*, 2001, **96**, 277–281.
12 X. W. Guo, X. P. Fang, Y. Sun, L. Y. Shen, Z. X. Wang and L. Q. Chen, *J. Power Sources*, 2013, **226**, 75–81.
13 X. Chen, K. Kierzek, K. Wilgosz, J. Machnikowski, J. Gong, J. Feng, T. Tang, R. J. Kalenczuk, H. Chen, P. K. Chu and E. Mijowska, *J. Power Sources*, 2012, **216**, 475–481.
14 B. P. Vinayan and S. Ramaprabhu, *J. Mater. Chem. A*, 2013, **1**, 3865–3871.
15 X. Li, X. Meng, J. Liu, D. Geng, Y. Zhang, M. N. Banis, Y. Li, J. Yang, R. Li, X. Sun, M. Cai and M. W. Verbrugge, *Adv. Funct. Mater.*, 2012, **22**, 1647–1654.
16 S. Ding, D. Luan, F. Y. C. Boey, J. S. Chen and X. W. Lou, *Chem. Commun.*, 2011, **47**, 7155–7157.
17 Y. Zhu, C. Li and C. Cao, *RSC Adv.*, 2013, **3**, 11860–11868.
18 Q. Han, J. Zai, Y. Xiao, B. Li, M. Xu and X. Qian, *RSC Adv.*, 2013, **3**, 20573–20578.
19 H. X. Yang, J. F. Qian, Z. X. Chen, X. P. Ai and Y. L. Cao, *J. Phys. Chem. C*, 2007, **111**, 14067–14071.
20 Y. J. Hong, M. Y. Son and Y. C. Kang, *Adv. Mater.*, 2013, **25**, 2279–2283.
21 S. J. Han, B. C. Jang, T. Kim, S. M. Oh and T. Hyeon, *Adv. Funct. Mater.*, 2005, **15**, 1845–1850.
22 W. Wei, Z. Wang, Z. Liu, Y. Liu, L. He, D. Chen, A. Umar, L. Guo and J. Li, *J. Power Sources*, 2013, **238**, 376–387.
23 M. Sevilla and A. B. Fuertes, *Chem.–Eur. J.*, 2009, **15**, 4195–4203.
24 M. Zheng, Y. Liu, K. Jiang, Y. Xiao and D. Yuan, *Carbon*, 2010, **48**, 1224–1233.
25 M. Zheng, Y. Liu, Y. Xiao, Y. Zhu, Q. Guan, D. Yuan and J. Zhang, *J. Phys. Chem. C*, 2009, **113**, 8455–8459.
26 M. Sevilla and A. B. Fuertes, *Carbon*, 2009, **47**, 2281–2289.
27 C. Yao, Y. Shin, L. Q. Wang, C. F. Windisch, Jr, W. D. Samuels, B. W. Arey, C. Wang, W. M. Risen, Jr and G. J. Exarhos, *J. Phys. Chem. C*, 2007, **111**, 15141–15145.
28 P. Manjula, R. Boppella and S. V. Manorama, *ACS Appl. Mater. Interfaces*, 2012, **4**, 6252–6260.
29 S. Y. Ho, A. S. W. Wong and G. W. Ho, *Cryst. Growth Des.*, 2009, **9**, 732–736.
30 Y. Zhao, J. Li, Y. Ding and L. Guan, *RSC Adv.*, 2011, **1**, 852–856.
31 K. Kravchyk, L. Protesescu, M. I. Bodnarchuk, F. Krumeich, M. Yarema, M. Walter, C. Guntlin and M. V. Kovalenko, *J. Am. Chem. Soc.*, 2013, **135**, 4199–4202.
32 S. K. Park, S. H. Yu, N. Pinna, S. Woo, B. Jang, Y. H. Chung, Y. H. Cho, Y. E. Sung and Y. Piao, *J. Mater. Chem.*, 2012, **22**, 2520–2525.
33 W. Wang, P. Li, Y. Fu and X. Ma, *J. Power Sources*, 2013, **238**, 464–468.
34 K. T. Nam, D. W. Kim, P. J. Yoo, C. Y. Chiang, N. Meethong, P. T. Hammond, Y. M. Chiang and A. M. Belcher, *Science*, 2006, **312**, 885–888.
35 X. Wang, X. Zhou, K. Yao, J. Zhang and Z. Liu, *Carbon*, 2011, **49**, 133–139.
36 W. Wei, W. Lv, M. B. Wu, F. Y. Su, Y. B. He, B. Li, F. Y. Kang and Q. H. Yang, *Carbon*, 2013, **57**, 530–533.
37 R. D. Cakan, M.-M. Titirici, M. Antonietti, G. Cui, J. Maier and Y.-S. Hu, *Chem. Commun.*, 2008, 3759–3761.
38 Z. T. Li, G. L. Wu, D. Liu, W. T. Wu, B. Jiang, J. T. Zheng, Y. P. Li, J. H. Li and M. B. Wu, *J. Mater. Chem. A*, 2014, **2**, 7471–7477.
39 Z. Wang, L. Zhou and X. W. Lou, *Adv. Mater.*, 2012, **24**, 1903–1911.

 This journal is © The Royal Society of Chemistry 2014